doi: 10.15407/ujpe61.06.0482

L. KERNAZHITSKY,[1] V. SHYMANOVSKA,[1] T. GAVRILKO,[1] V. NAUMOV,[1]
L. FEDORENKO,[2] V. KSHNYAKIN,[3] A. BURTSEV,[4] J. BARAN[5]

[1] Institute of Physics, Nat. Acad. of Sci. of Ukraine
(46, Prosp. Nauky, Kyiv 03028, Ukraine; e-mail: kern@iop.kiev.ua)
[2] V.E. Lashkaryov Institute of Semiconductor Physics, Nat. Acad. of Sci. of Ukraine
(45, Prosp. Nauky, Kyiv 03028, Ukraine)
[3] Sumy State University
(2, Rymsky-Korsakov Str., Sumy 40007, Ukraine)
[4] G.V. Kurdyumov Institute for Metal Physics, Nat. Acad. of Sci. of Ukraine
(36, Academician Vernadsky Blvd., Kyiv 03680, Ukraine)
[5] Institute of Low Temperature and Structure Research, Polish Academy of Sciences
(2, Okolna Str., 50-950 Wroclaw, Poland)

PACS 61.72.Uj, 71.55.Eq,
78.40.Fy, 78.55.Et

EFFECT OF Cr-DOPING ON LUMINESCENCE OF NANOCRYSTALLINE ANATASE TiO_2 POWDERS

We have studied the photoluminescence (PL) of titanium dioxide nanocrystalline powders (TiO_2) synthesized by the thermal hydrolysis in the form of anatase (A), whose surface has been modified by the adsorption of chromium ions (Cr^{3+}). The samples are characterized by X-ray diffraction, X-ray fluorescence, and Raman spectroscopy. PL spectra were excited by a nitrogen UV laser. The Cr^{3+} ion doping in A/TiO_2 leads to short-wave and long-wave shifts of the PL peaks due to the Burstein–Moss effect and due to the contribution of radiation "tails" of the electron density of states, respectively. The PL intensity of Cr^{3+}-doped A/TiO_2 at low concentration of Cr^{3+} (up to 0.5 at.%) increases in comparison with the undoped A/TiO_2 due to the formation of additional centers of radiative recombination of carriers. With increasing the concentration of Cr^{3+} (∼1.0 at.%), the A/TiO_2 PL intensity decreases due to the concentration quenching.

Keywords: titanium dioxide, anatase, Cr-doping, photoluminescence.

1. Introduction

In recent few decades, titanium dioxide (TiO_2) was extensively studied by different research centers throughout the world due to its wide applications in such areas as photocatalysis, solar energy conversion, gas sensing, and others [1–4]. Anatase (A) is known as one of the two main crystalline structures of TiO_2, which transform into the rutile phase on heating. It is recognized that the photoresponse of A/TiO_2 can be extended to the visible light region by the cation doping. Anpo *et al.* [5] reported that the doped metal ions exhibit an isomorphic replacement of Ti^{4+} ions in the TiO_2 crystal lattice and decrease the band gap energy enabling TiO_2 to absorb under visible light. Transition ion dopants may also act as trapping centers, at which excited electrons may recombine with holes, by varying the lifetime of the generated charge carriers [6].

Several methods like sol-gel [7], ion implantation [8], and hydrothermal doping method [9] implying the incorporation of ions of doping transition metals into a TiO_2 network have been employed to improve the photophysical properties of TiO_2 in order to make the material more sensitive and to extend its spectral

Characterization of *A*-TiO_2 prepared samples

Sample	T, °C	Phase composition	Cr contents, % at. (XRF)	D_{hkl}, nm (XRD)	O/Ti stoichiometry and crystallite sizes, d (nm) (Raman)
$A1$	200	A-100%	0	16.2 (101)	O/Ti = 1.995, $d = 14$
$A2$	300	A-100%	0	9.8 (101)	O/Ti = 1.983, $d = 8.3$
$A2$/Cr-1	300	A-100%	0.54	14.7 (101)	O/Ti = 1.994, $d = 12.2$
$A2$/Cr-2	300	A-100%	0.98	10.0 (101)	O/Ti = 1.986, $d = 9.4$

response toward the visible spectral range. In our research, the samples of the single-phase A/TiO_2 were chemically modified with Cr^{3+} ions by the adsorption from aqueous solutions of $CrCl_3$. This surface doping technique differs completely from that of the substitution of ions at the Ti sites. In the above-mentioned methods, dopants mainly affect the carrier traps in bulk, wheras they acts, at the surface doping technique, mostly on the surface traps. Considering that photoluminescence (PL) spectroscopy is a highly sensitive tool to study the photophysics of the photogenerated species in semiconductor materials, we apply this method in this paper to undoped and Cr-doped nanocrystalline A/TiO_2 samples.

In this paper, we have synthesized a nanocrystalline TiO_2 powder surface-doped with two different concentrations of Cr ions (0.5 and 1% at.) in A/TiO_2 by the adsorption from $CrCl_3$ solutions. Room-temperature PL spectra of the samples are measured to obtain information about the emission peaks associated with excitons and surface and oxygen defects. Effects of Cr doping on the PL behavior of the nanocrystalline A/TiO_2 powders are studied in details. This study may contribute to the deeper understanding of the doping effect on the photoluminescence properties of TiO_2.

2. Experimental

2.1. Preparation of samples

Nanocrystalline pure TiO_2 with anatase crystal structure was synthesized at 100 °C in the presence of colloidal titanium nuclei of the anatase crystal form [10]. The process takes place in a very acidic environment (hydrochloric acid solution), which prevents the adsorption of impurities on titanium hydroxide during the synthesis. The detailed description of the synthesis procedure was reported in our previous work [11]. Afterward, the obtained pure A/TiO_2 powders were chemically modified with Cr^{3+} cations by the adsorption from $CrCl_3$ aqueous solutions. The reaction mixture was stirred for 24 h at room temperature to reach the sorption equilibrium. The obtained sediment was filtered, dried at 150 °C for 5h, carefully washed with bi-distilled water till the disappearance of impurities in the filtrate. After the heating, the pure nanocrystalline TiO_2 powders were annealed at 200 °C ($A1$) and 300 °C ($A2$) in air for 8 h. Finally, the surface-doped TiO_2 samples with Cr contents of 0.54 at.% (denoted as $A2$/Cr-1) and 0.98 at.% ($A2$/Cr-2) were annealed at 300 °C in air for 8 h too. The characteristics of the prepared *A*-TiO_2 samples are given in the Table.

2.2. Experimental methods

The XRD patterns of pure and Cr^{3+}surface-doped A TiO_2 samples were obtained with a DRON-2 X-ray diffractometer under high-intensity $Co_{K\alpha}$(0.179 nm) radiation. The mean crystallite size of A TiO_2 samples was evaluated from the A (101) characteristic peak using the Debye–Scherrer formula:

$$D = K\lambda/\beta\cos\theta,$$

where D is the mean crystallite size in angstroms, K is a constant, which is taken here to be 0.89, λ is the X-ray radiation wavelength, β is the full width at half-maximum (FWHM) of the diffraction peak, and θ is the diffraction angle.

The chemical composition of TiO_2 samples was identified by the X-ray fluorescence (XRF) analysis, by using an XNAT-Control instrument. The measurement errors for the XRF data did not exceed ±5%.

A scanning electron microscope JEOL JSM 6490 (SEM) equipped with an energy dispersive X-ray spectrometer (EDS) was used to observe the morphologies of samples and for the elemental analysis.

The FT-Raman spectrum was recorded at room temperature, by using the 1064-nm line of a Nd:YAG laser with the excitation wave length in the region

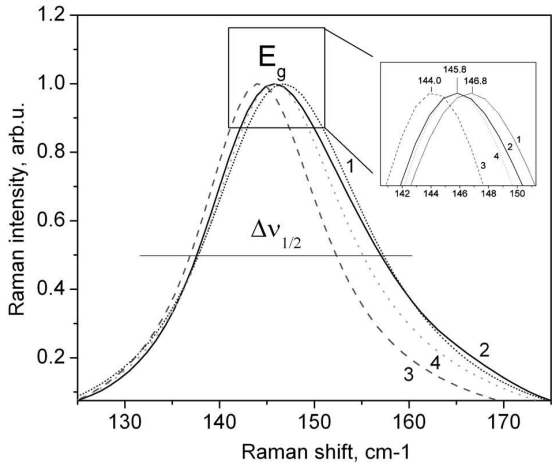

Fig. 1. E_g vibrational mode for *1* – *A*1, *2* – *A*2, *3* – *A*2/Cr-1, *4* – *A*2/Cr-2

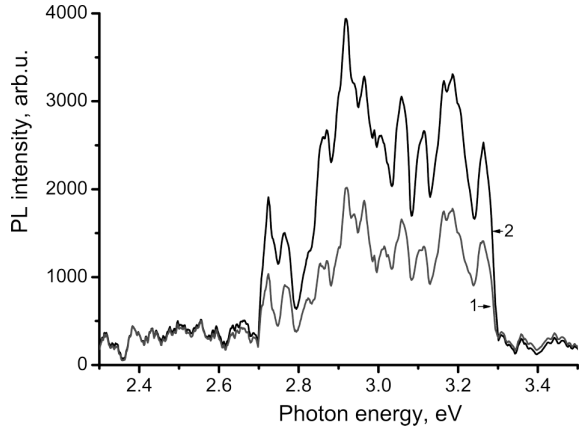

Fig. 2. PL spectra for nondoped TiO_2 anatase samples: *1* – *A*1; *2* – *A*2

50–4000 cm^{-1} on a Bruker IFS 88 equipped with an FRA-106 FT-Raman attachment and a liquid-nitrogen-cooled Ge detector. 128 scans were accumulated at 2 cm^{-1} resolution at a laser power of 300 mW.

PL spectra measurements were carried out using a portable multichannel optical spectrum analyzer Solar SL40-2 (3648-pixel CCD sensor TCD 1304 AP, diffraction grating 600 l/mm, spectral resolution ∼0.3 nm, and registration time ∼7 ms) in the spectral range of 220–750 nm. PL spectra of *A* TiO_2 samples were excited by a pulsed N_2-laser (λ_{ex} = 337.1 nm, 50 μJ pulse energy, 7-ns pulse duration, 50-Hz repetition rate, beam aperture of ∼3 mm). A special optical interference filter was used to discriminate the laser light and the laser-induced luminescence. PL was measured in the back scattering configuration. All measurements were carried out at room temperature.

3. Results and Discussion

3.1. XRD analysis

According to the XRD characterization (Table), the prepared *A*1 and *A*2 TiO_2 samples have a well crystallized pure-phase structure. The mean sizes of nanocrystallites in polydisperse *A* TiO_2 powders, which were determined from XRD patterns under $Cu_{K\alpha}$ irradiation, appeared to be equal to 16.2 and 9.8 nm for *A*1 and *A*2 samples, respectively (see Table). According to the XRD results, the obtained samples are only the single-phase anatase TiO_2. No chromium oxide impurity phase was detected. XRD patterns from Cr^{3+} surface-doped TiO_2 samples were identical to those from pure TiO_2. The crystallite size was estimated from the FWHM of the (101) plane of anatase to be equal to 14.7 nm and 10.0 nm for *A*2/Cr-1 and *A*2/Cr-2 samples, respectively.

The room-temperature FT-Raman spectra of the prepared nanocrystalline TiO_2 are typical of the TiO_2 anatase crystalline phases (Fig. 1), allowing us to assign the observed bands to certain types of TiO_2 lattice vibrations [12, 13]. The position (ν_{max}) of the low-frequency E_g vibrational mode (143 cm^{-1} for A) and its half- width ($\Delta\nu_{1/2}$) are known to be very sensitive to the stoichiometric ratio (O/Ti) and the TiO_2 crystallites size [14]. Based on the FT-Raman measurement of E_g peak positions and half-width (Fig. 1), the stoichiometry of the prepared TiO_2 samples were determined (Table).

3.2. Room-temperature laser-excited luminescence

PL spectra of undoped *A* TiO_2 samples excited with a pulsed N_2 laser (λ_{ex} = 337.1 nm) are shown in Fig. 2. As is seen, the laser-induced PL emission spectrum of the *A*/TiO_2 samples consists of a broad PL band showing a well-resolved fine structure. As we have previously reported [15], such well-resolved PL structure is usually recorded for polydispersed TiO_2 samples at a sufficiently high intensity of the exciting light. In our measurements, the N_2-laser intensity per pulse was higher enough (up to 4.4×10^{10} Wcm^{-2}). So, we were able to register the UV emission peaks at 3.03–3.25 eV (408–381 nm); one dominant violet peak at 2.91 eV (425 nm) along with less prominent peaks at 2.84–3.00 eV (436–413 nm) in this region;

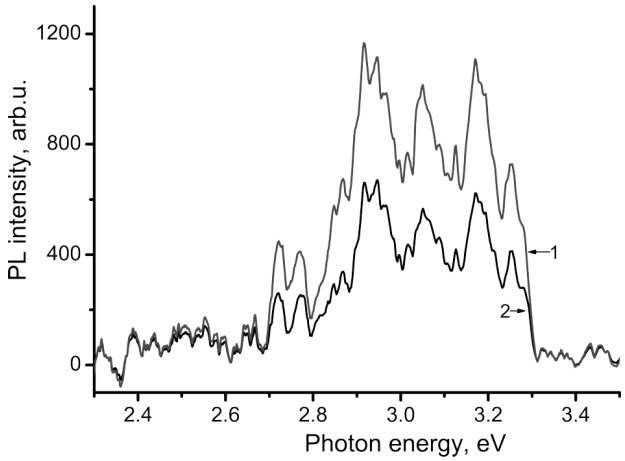

Fig. 3. PL spectra for Cr surface-doped A/TiO_2 samples: *1* – $A2$/Cr-1; *2* – $A2$/Cr-2

and two peaks at 2.71–2.76 eV (457–447 nm). As we have shown in the previous work [15], the PL fine structure in 2.7–3.0 eV spectral range arises as a result of the strong exciton-phonon interaction in TiO_2 under the high-power N_2-laser excitation.

The appearance of the UV emission peaks in the PL spectra of TiO_2 is generally attributed to the band-to-band transitions in TiO_2. As we have earlier found [15], the PL peak at 3.26 eV in anatase corresponds to the band edge transition with band gap value of 3.29 eV for A/TiO_2. Other emission peaks observed in the PL spectra of anatase TiO_2 (Fig. 2) at 3.05 eV (406 nm), 3.08 eV (402 nm), 3.17–3.19 eV (391–388 nm), and 3.24 eV (382 nm) can be ascribed to indirect allowed transitions [16]. The strong emission peak at 2.91 nm (425 nm) in the A/TiO_2 PL spectra is ascribed to the recombination of self-trapped excitons (STE) in anatase [17]. The emission peaks near 2.71–2.76 eV (457–447 nm) PL are attributed to the defect centers originated by trapping two electrons in the oxygen vacancies (F-center) [18].

The PL emission from $A2/TiO_2$ sample calcined at 300 °C is higher compared to that of $A1$ calcined at 200 °C. This can be explained by the influence of the crystallite size on the value of PL intensity. In our case (see Table), the crystallite size for $A2/TiO_2$ is less, and the O/Ti stoichiometry is smaller than for $A1/TiO_2$. This leads to the increase in the number of surface defect states and oxygen vacancies and in the surface hydration degree, which leads to the increased exciton formation and the corresponding en-

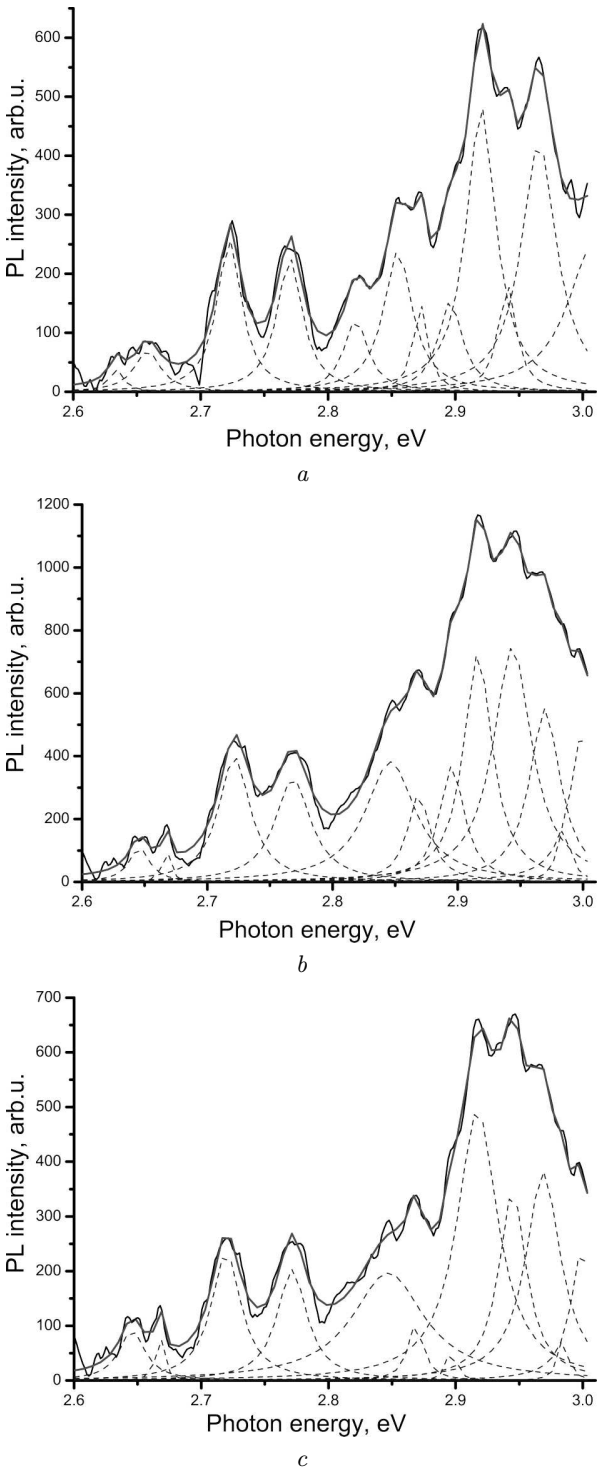

Fig. 4. PL spectra for pure and Cr surface-doped A/TiO_2 samples in the visible region: $A2$, $r^2 = 0.9936$ (*a*); $A2$/Cr-1, $r^2 = 0.9965$ (*b*); $A2$/Cr-2, $r^2 = 0.9939$ (*c*)

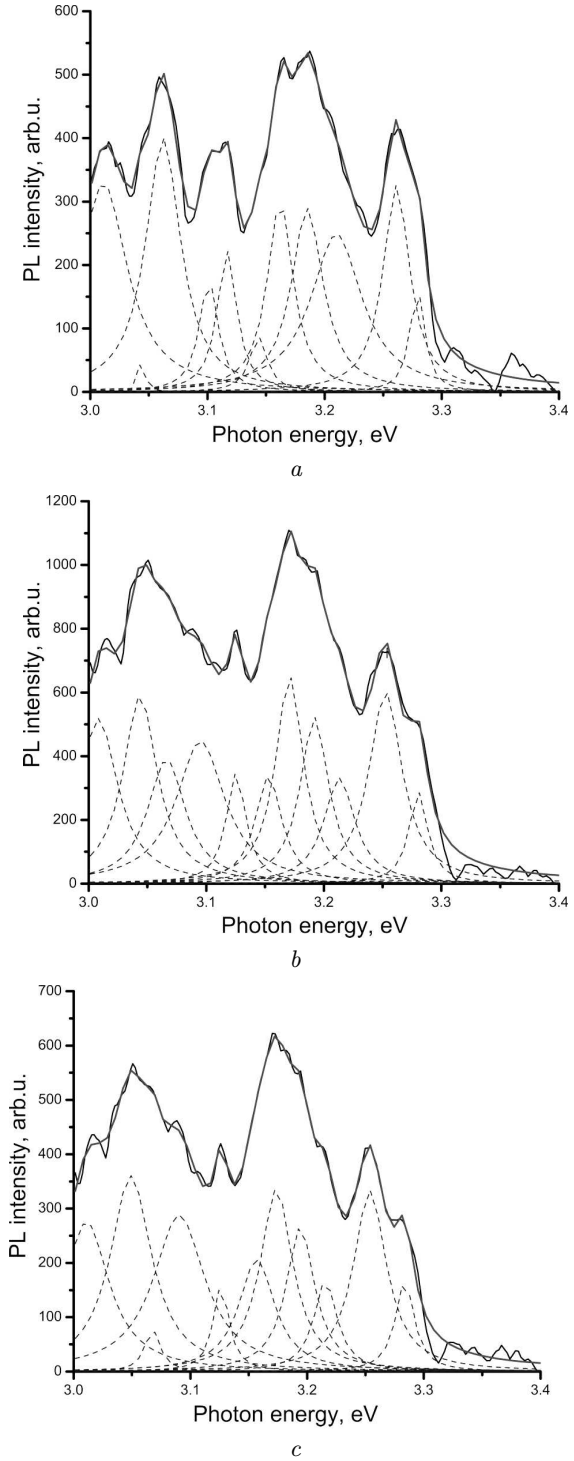

Fig. 5. PL spectra for pure and Cr surface-doped A/TiO_2 samples in the UV region: $A2$, $r^2 = 0.9936$ (*a*); $A2$/Cr-1, $r^2 = 0.9949$ (*b*); $A2$/Cr-2, $r^2 = 0.9951$ (*c*)

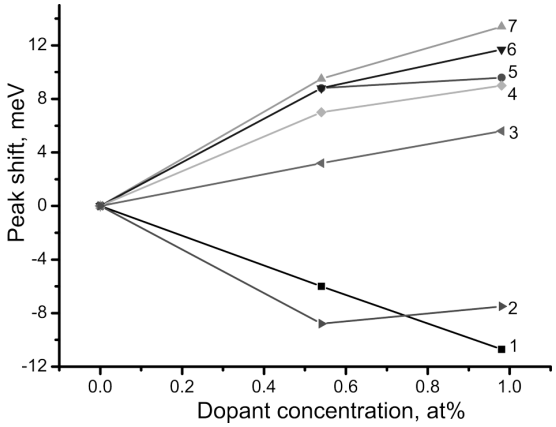

Fig. 6. Shifts of PL peaks in a doped$A/Cr\ TiO_2$: *1* – 3.10 eV; *2* – 3.26 eV; *3* – 3.21 eV; *4* – 3.18 eV; *5* – 3.11 eV; *6* – 3.16 eV; *7* – 3.14 eV

hancement of a PL signal [19]. Cr-doped TiO_2 samples exhibit PL spectra with a similar curve shape, while the intensity of PL spectra of Cr-doped A samples varied (Fig. 3).

For a more thorough study of the PL complex structure, the emission peaks were Lorentz-fitted with a correctness r^2 separately in the visible region (2.8–3.0 eV) and in the UV region (3.0–3.3 eV). As can be seen from the Lorentz decomposition of the PL spectrum in the visible region of 2.8–3.0 eV (Fig. 4, *a*, *b*, *c*), the position of all peaks in the samples of doped anatase are not changed practically in comparison with the undoped one. The contribution to the own Cr^{3+} emission in A/TiO_2 (Fig. 4, *b*, *c*) leads to a certain broadening of the peaks in the region of 2.71–2.77 eV (457–447 nm) and to a redistribution of the intensities of the peaks.

As for pure anatase (Fig. 5, *a*), 12 peaks ($r^2 = 0.9936$) can be seen. The peaks at 3.06, 3.10, 3.16, and 3.19 eV correlate well with the spectral features observed in the absorption spectrum of anatase [11]. When anatase is doped with chromium (Fig. 5, *b*, *c*), the number of peaks remains the same. However, there is a shift of the PL peaks near the edge of the fundamental band gap for $A2$/Cr-1 and $A2$/Cr-2 samples.

As is seen (Fig. 6), there are shifts of the peaks to shorter and longer wavelengths. The shift is proportional to the concentration of Cr ions. The maximum blue shift of about 12 meV is observed for the peak at 3.14 eV. The reverse red shift of about 10 meV is observed for the peak at 3.25 eV.

It is known that the strong doping of a semiconductor may lead to a change in the band structure [20]. One such effect is to reduce the band gap due to the formation of "tails" of the electron density of states that is a result of the non-equilibrium distribution of impurities. Another important phenomenon, which occurs in the case of heavily doped semiconductors, is a phenomenon of the increase in the energy of interband transitions due to the filling of the conduction band by free electrons, which is called the Burstein–Moss effect [21].

It should be noted that these two effects compete with each other. So, we observed short- and long-wave shifts in PL spectra of doped TiO_2 samples, which can be attributed to the Burstein–Moss effect and the contribution of "tails" of the density of electronic states, respectively.

As can be seen from the PL spectra of anatase TiO_2 (Fig. 2, 3), the intensity of the emission peaks of band-to-band, band edge and exciton luminescence, which is associated with defective states, are changed for chromium-doped samples. To understand such difference, we have plotted a normalized intensity ratio (I) of the peaks in the UV and violet spectral regions to the intensity of the 2.72 eV peak ($I_{2.72}$) in the visible spectral region. Figure 7 shows such dependences for the band-to-band UV emission peaks at 3.06 eV (BB1), 3.12 eV (BB2), and 3.17 eV (BB3) and the band edge (BE) emission peak at 3.26 eV, as well as the STE emission peak centered at 2.91 eV.

It was found that the $I/I_{2.72}$ intensity ratios firstly increase at a low Cr content (∼0.5 at.%) and then slightly decrease for a higher Cr content (∼1 at.%). This effect is commonly known as the concentration quenching [22]. As known [23], in pure TiO_2 nanocrystallites, the oxygen vacancies and other defects act as luminescence enhancers and increase the emission intensity, as compared to a TiO_2 bulk crystal. Doping with Cr cations generates additional recombination centers, which may act either as luminescence enhancers or quenchers. The other factor affecting the PL intensity is the mobility of carriers [24]. The dopants and the defects present in the bulk, grain boundaries, and on the surface reduce the mobility of free carriers. The mobile carriers are scattered, when they approach charged dopants or defects. A decrease in the mobility increases the separation of the carriers, by limiting their recombination. Hence, the PL emission decreases. We assume that, at a low Cr concentration (0.5 at.%), doping leads to the formation of additional radiative recombination centers in anatase TiO_2; so, the PL emission intensity increases. The higher Cr content (1.0 at.%) causes a decrease in the mobility of carriers and an increase in the amount of nonradiative recombination centers, which leads to a decrease in the PL intensity. Note that Cr-doping has little effect on the BE emission intensity for anatase TiO_2 samples.

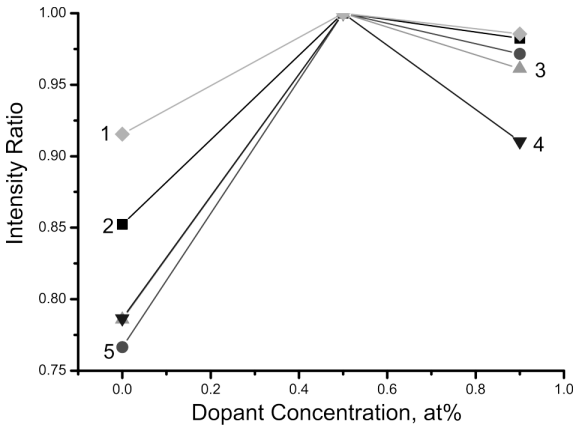

Fig. 7. Normalized intensity ratio of BE, BB1, BB2, BB3, and STE emission peaks related to the oxygen defect emission peak at 2.72 eV for undoped and Cr-doped A TiO_2: *1* – BE (3.26 eV); *2* – STE (2.91eV); *3* – BB1 (3.06 eV); *4* – BB2 (3.12 eV); *5* – BB3 (3.17 eV)

4. Conclusions

Thus, we have studied the effect of surface Cr-doping on the PL and UV–vis absorption spectra of nanocrystalline anatase TiO_2 synthesized by the thermal hydrolysis. The excitonic and band-to-band luminescences of nanocrystalline A/Cr TiO_2 are observed, by using the high-intensity N_2 laser excitation at room temperature. A detailed analysis of the A/Cr TiO_2PL emission spectra is carried out. The observed blue and red shifts of the PL peaks in A/Cr TiO_2 are due to the Burstein–Moss and band tailing effects, respectively. The nonmonotonic change in the intensity of UV and violet PL emission peaks compare to the visible PL peak in A TiO_2 is explained by the concentration quenching effect after the Cr doping.

The work was supported by the National Academy of Sciences of Ukraine under the Research Program "Nanophysics and Nanoelectronics" (Project No. VC-157).

1. A. Fujishima, X. Zhang, and D.A. Tryk, Surf. Sci. Rep. **63**, 515 (2008).
2. Arafat C. Xu, J. Wu, U.V. Desai, and D. Cao, Nano Lett. **12**, 2420 (2012).
3. M.I. Baraton, Recent Pat. Nanotechnol. **6**, 10 (2012).
4. M.M. Arafat, B. Dinan, S.A. Akbar, and A.S.M.A. Haseeb, Sensors **12**, 7207 (2012).
5. H. Yamashita, M. Harada, J. Misaka, M. Takeuchi, K. Ikeue, and M. Anpo, J. Photochem. Photobiol. A **148**, 257 (2002).
6. W.Y. Choi, A. Termin, and M.R. Hoffmann, Angew. Chem. Int. Ed. **33**, 1091 (1994).
7. B. Choudhury and A. Choudhury, Mater. Chem. Phys. **132**, 1112 (2012).
8. M. Anpo and M. Takeuchi, J. Catal. **216**, 505 (2003).
9. J. Zhu, Z. Deng, F. Chen, J. Zhang, H. Chen, M. Anpo, J. Huang, and L. Zhang, Appl. Catal. B-Environ. **62**, 329 (2006).
10. V.V. Shymanovskaya, A.A. Dvernyakova, and V.V. Strelko, Izv. Akad. Nauk. SSSR, Neorg. Mater. **24**, 1188 (1988).
11. L. Kernazhitsky, V. Shymanovska, T. Gavrilko, V. Naumov, V. Kshnyakin, and T. Khalyavka, J. Solid State Chem. **198**, 511 (2013).
12. S.P.S. Porto, P.A. Fleury, and T.C. Damen, Phys. Rev. **154**, 522 (1967).
13. J.C. Parker and R.W. Siegel, Appl. Phys. Lett. **57**, 943 (1990).
14. W.F. Zhang, Y.L. He, M.S. Zhang, Z. Yin, and Q. Chen, J. of Phys. D: Appl. Phys. **33**, 912 (2000)
15. L. Kernazhitsky, V. Shymanovska, T. Gavrilko, V. Naumov, V. Kshnyakin, and J. Baran, J. Lumin. **146**, 199 (2014).
16. N. Daude, C. Gout, and C. Jouanin, Phys. Rev. B **15**, 3229 (1977).
17. H. Tang, H. Berger, P.E. Schmid, and F. Levy, Solid State Comm. **92**, 267 (1994).
18. U. Hormann, U. Kaiser, M. Albrecht, J. Geserick, and N. Husing, J. Phys. Conf. Ser. **209**, 012039 (2010).
19. J. Liqiang, Q. Yichun, W. Baiqi, L. Shudan, J. Baojiang, Y. Libin, F. Wei, F. Honggang, and S. Jiazhong, Solar Energy Mater. and Solar Cells **90**, 1773 (2006).
20. H.C. Casey, jr., and F. Stern, J. Appl. Phys. **47**, 631 (1976).
21. E. Burstein, Phys. Rev. **83**, 632 (1954).
22. R. Chen, J.L. Lawless, and V. Pagonis, Radiation Measur. **46**, 1380 (2011).
23. N. Serpone, J. Phys. Chem. B **110**, 24287 (2006).
24. X.B. Wang, C. Song, K.W. Geng, F. Zeng, and F. Pan, Appl. Surf. Sci. **253**, 6905 (2007).

Received 23.09.15

Л. Кернажицький, В. Шимановська,
Т. Гаврилко, В. Наумов, Л. Федоренко,
В. Кшнякин, В. Бурцев, Я. Баран

ВПЛИВ ДОМІШКИ ХРОМУ
НА ЛЮМІНЕСЦЕНЦІЮ НАНОКРИСТАЛІЧНИХ
ПОРОШКІВ АНАТАЗУ TiO_2

Р е з ю м е

Наведено результати комплексного дослідження нанокристалічних полідисперсних зразків TiO_2, синтезованих методом термічного гідролізу у формі чистого анатазу, поверхню яких було модифіковано іонами хрому шляхом адсорбції з розчинів $CrCl_3$. Зразки було досліджено методами рентгенівської дифракції, рентгенівської флуоресценції, спектроскопії комбінаційного розсіювання світла, оптичного поглинання та фотолюмінесценції (ФЛ). Спектри ФЛ вивчали при збудженні TiO_2 інтенсивним УФ випромінюванням азотного лазера з довжиною хвилі збудження 337,1 нм (3,68 еВ) при кімнатній температурі. Показано, що інтенсивність люмінесценції допованого анатазу залежить від концентрації хрому: при малих концентраціях (0,5 at.%) вона зростає у порівнянні з чистим TiO_2 внаслідок появи додаткових центрів рекомбінації зарядів, а при великих ($\sim$1,0 at.%) – падає внаслідок концентраційного гасіння. В спектрах ФЛ спостерігалися короткохвильовий та довгохвильовий зсуви смуг крайового випромінювання допованих зразків TiO_2, які було віднесено до ефекту Бурштейна–Мосса та внеску радіаційних "хвостів" густини електронних станів, відповідно.